Journal of Applied Physics TUTORIAL pubs.aip.org/aip/jap

Tutorial: Defects in topological semimetals

Cite as: J. Appl. Phys. **136**, 091102 (2024); doi: 10.1063/5.0217533
Submitted: 5 May 2024 · Accepted: 4 August 2024 ·
Published Online: 5 September 2024

Kirstin Alberi,[1,2,a)] Chase Brooks,[3] Ian Leahy,[1] and Stephan Lany[1]

AFFILIATIONS

[1]National Renewable Energy Laboratory, Golden, Colorado 80401, USA
[2]Renewable and Sustainable Energy Institute, National Renewable Energy Laboratory and University of Colorado, Boulder, Colorado 80301, USA
[3]Department of Physics, University of Colorado, Boulder, Colorado 80309, USA

Note: This paper is part of the special topic, Defects in Semiconductors 2024.
[a)]**Author to whom correspondence should be addressed:** Kirstin.Alberi@nrel.gov

ABSTRACT

Three-dimensional topological semimetals are a class of electronic materials in which their bulk and surface states contain linear band touching nodes near the Fermi level. Like semiconductors, their properties will be affected by point and extended defects in their crystal structures, although the extent to which defects and disorders influence topological semimetals may differ in key ways due to their unique electronic structures. In this Tutorial, we provide an overview of the defects in topological semimetals, covering both computational and experimental methods for exploring defect-property relationships. We also include a discussion on open questions that still need to be explored further.

I. INTRODUCTION

Advancing a material from discovery to application requires an understanding of how to manipulate its behavior through intentional changes to its structure and composition as well as the associated consequences of unintended deviations. Mastery of defects and impurities in semiconductors, in particular, has proven to be a critical factor in realizing many of the technologies that are now ubiquitous in the age of electronics (i.e., transistors, solar cells, light-emitting diodes, and lasers). This success was achieved under dual efforts to understand and control their impact on electron transport and recombination. Some aspects are beneficial for device design, including the use of dopants to intentionally tune the Fermi level and crystalline point defects to manipulate electron spin. Other aspects are detrimental. For example, defects can play a role in increasing non-radiative recombination and lowering electron mobility. As we now explore newer classes of electronic materials to extend device functionality, we will need to translate this mastery to them.[1]

Recently, topological semimetals (TSMs) have emerged as a promising addition to the larger collection of quantum materials, in which quantum mechanics profoundly shapes their behavior.[2] Topologically, non-trivial materials have distinct band structures from conventional (trivial) semiconductors and insulators that result from their bonding arrangement, the presence of large spin–orbit coupling, and the retention of specific symmetries.[3–5] Existing at the boundary between topological and trivial insulators, TSMs are characterized by the presence of linear band touching nodes in their bulk and surface states near the Fermi level. The details of node arrangements can differ slightly, leading to several different classes of TSMs. Dirac semimetals exhibit both inversion and time reversal symmetries and contain degenerate band touching nodes, while Weyl semimetals lack either inversion or time reversal symmetry and exhibit chiral nodes that are separated in momentum and/or energy space. A third class of TSMs, known as nodal line semimetals, exhibit bands that cross in a line rather than a point.

The distinct band structures of these materials confer a number of interesting properties.[3,4] First and foremost, linear band dispersions near the Fermi level give way to massless (or very low mass) Dirac and Weyl fermions. Here, we will still use the terminology of electrons and holes to denote these charged carriers, in keeping with precedent in the literature. The band structure additionally protects against quasiparticle backscattering. As a consequence, they typically have high mobilities when the Fermi level lies near the band touching nodes. A second feature specific to

Weyl semimetals is that the nodes (and associated Weyl fermions) are chiral. This feature has the potential to support chiral anomaly, wherein parallel electric and magnetic fields can cause Weyl fermions to be pumped predominantly to the Landau levels of one chirality and, therefore, generate an excess population of spin-polarized fermions. Overall, TSMs can exhibit anomalous charge carrier transport and non-linear optical responses that may be advantageous for a variety of electronic and optoelectronic devices, including spintronics and photodetectors.

The push to incorporate TSMs into devices will undoubtedly require a level of effort to understand and control defects and impurities similar to that allocated to semiconductors. Like semiconductors, TSM crystals will contain a variety of point and extended defects that depend on their propensity to form thermodynamically as well as the details of their synthesis. Defects and impurities also have the potential to influence transport behavior in beneficial and detrimental ways. While much of our knowledge of defects in semiconductors can serve as a foundation for predicting their formation and behavior in TSMs, nuances also arise as a result of their non-trivial band structures. For example, backscattering may be forbidden, but defects may influence fermion scattering in other ways depending on their energy levels and the strength and spatial extent of the potentials they introduce. In addition to the potentially negative impact on carrier mobility, scattering has also been observed to introduce large and/or negative linear magnetoresistance (MR), which may be beneficial for device design.[6] Furthermore, the necessary formation of defect states within the bands has an impact on their formation energies.

Given these nuances, the intent of this Tutorial is to provide an overview of what is currently known about the defects in TSMs. It will include a theoretical framework for calculating defect formation energies, experimental methods for detecting defects, and the role of defects on the Fermi level and carrier transport. Finally, it highlights knowledge gaps that must still be filled to position TSMs for device applications.

II. CONCEPTUAL VIEW OF DEFECTS IN TOPOLOGICAL SEMIMETALS

First-principles calculations of point defects using the method of periodic supercells have been adopted and modified for TSMs. These methods and their limitations are well understood for bandgap systems,[7,8] where supercell calculations can be limited by nonphysical interactions between the defect being calculated and its periodic images, and where corrections are necessary to extrapolate formation energies to a dilute defect limit. However, in the prototypical Dirac TSM Cd_3As_2, the relevant formation energies deviate significantly from the dilute limit, requiring a tailored approach for the capability to predict defect equilibria with temperature-dependent defect and charge carrier concentrations.[9]

Despite the absence of a bandgap, electrically active point defects (either intrinsic defects or dopants or impurities) in TSMs can be categorized into one of the two types of behavior, resembling "deep" and "shallow" levels in semiconductors.[10] The first kind are those that introduce localized defect states close to the energy E_{DP} of the Dirac point, within a range of accessible Fermi levels (E_F). These defects can form in different charge states depending on the occupation of the state as a function of E_F and, therefore, exhibit a tendency to pin the Fermi level. The other class of defects are those that do not introduce a localized state near E_F and, instead, release the carriers (electrons or holes for donor- or acceptor-like defects, respectively) into the band continuum, thereby also shifting the Fermi level.

Figure 1 shows the density of states (DOS) for select intrinsic and extrinsic defects in Cd_3As_2 and how they compare to the 80-atom defect-free primitive cell. The shape of the DOS illustrates the two distinct defect behaviors described above. The cadmium interstitial Cd_i, Cd vacancy V_{Cd}, and the substitution of tin on arsenic Sn_{As} all introduce delocalized electrons or hole carriers, raising or lowering the supercell Fermi level while the DOS of the Cd_3As_2 host is only moderately perturbed by the presence of the defect (especially when considering the high defect concentration implied by the limited supercell size). Thus, the supercell DOS exhibits a metallic behavior with E_F residing in the band continuum in these cases. In contrast, the V_{As} and Sn_{Cd} defects

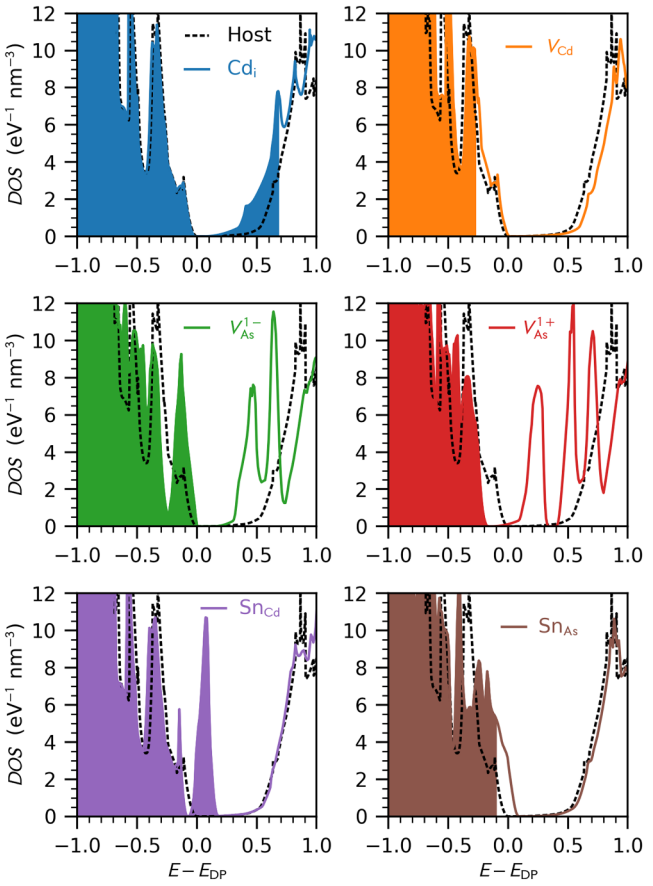

FIG. 1. Host and defect/dopant density of states (DOS) in Cd_3As_2 calculated with the SCAN functional (including spin-orbit coupling) as a function of energy E measured with respect to the Dirac point E_{DP}. Only the lowest energy Wyckoff positions are shown for each defect.

exemplify the case of localized defect states in the vicinity of the Dirac point. Specifically, V_{As} exhibits amphoteric behavior where a doubly degenerate defect state can be either occupied or unoccupied, corresponding to the negative V_{As}^{-1} charge state with a defect-induced spike in the DOS at −0.1 eV and to the positive V_{As}^{+1} with a defect state at +0.2 eV, respectively (see Fig. 1). Similarly, the neutral Sn_{Cd} causes a defect-localized state just above E_{DP}.

Due to the possibility of occupation changes, the defects with localized states give rise to charge transition levels much like in the case of semiconductors and insulators, except that they occur inside the band continuum instead of within the bandgap. This means that the preferred charge state can change as E_F varies with the presence of other electrically active defects and with the changes in temperature. In semiconductors, the defects without localized states are, nevertheless, able to bind carriers in a "shallow" effective mass-like level,[11] where the defect state essentially represents an envelope function of the "perturbed host state."[10] Due to the absence of a bandgap and the corresponding screening of the electrostatic potential, this type of bound state does not exist in a semimetal. Instead, as discussed below by way of quantitative calculations in Cd_3As_2, defects of this kind, including Cd_i, V_{Cd}, and Sn_{As}, are more appropriately viewed as charged defects being compensated by continuum carriers (or other defects of opposite charge).

III. COMPUTATIONAL DEFECT EQUILIBRIA

A. Theoretical framework

Within the well-established supercell approach,[7,8,12] the formation energy of a defect D in charge q is given by

$$\Delta H_{D,q}\left(E_F, \{\mu\}\right) = [E_{D,q} - E_h] + \sum_\alpha n_\alpha \mu_\alpha + qE_F, \quad (1)$$

where $E_{D,q}$ and E_h are the total energies of the defect and host supercells, respectively, μ_α are the chemical potentials of atom species α that are removed ($n_\alpha = +1$) or added ($n_\alpha = -1$) to the material in forming the defect. Importantly, when Eq. (1) is used for the prediction of defect concentrations, E_F must represent the thermodynamic, temperature-dependent electron chemical potential resulting from the complete defect equilibrium, rather than the zero-temperature Fermi level as obtained in the calculation of a single defect (cf. Fig. 1).

The straightforward calculation of the formation energies of the charge-neutral Cd_i and V_{Cd} defects, without specific consideration of the possible charge exchange between the defect and the DOS of the Cd_3As_2 host, exhibits a strong dependence on the size of the supercell used in the calculation,[9] as shown in Fig. 2. This observation correlates with the concentration-dependent shift of E_F, suggesting that these defects behave more like charged defects ($q \neq 0$), whose formation energies depend explicitly on E_F [see Eq. (1)]. In contrast, true "neutral" defects, such as the V_O^0 oxygen vacancy in ZnO,[7] typically exhibit only weak size and concentration dependencies.

To test the equivalence of the concentration-dependent formation energies of the charge-neutral defects and the respective

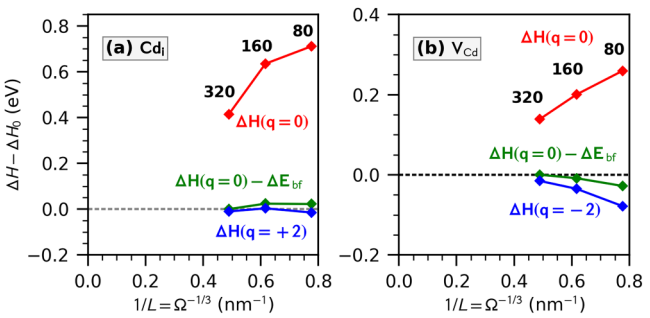

FIG. 2. The supercell size dependence of the formation energy ΔH of the (a) Cd_i and (b) V_{Cd} defects in Cd_3As_2 as a function of inverse linear supercell size $1/L = \Omega^{-1/3}$ obtained from supercell volume Ω. ΔH_0 corresponds to the dilute limit of the formation energy.[9]

formation energies of the charged defects in the presence of continuum carriers, the so-called "band-filling" energies are evaluated as[9,13]

$$\Delta E_{bf} = \sum_{\substack{n,\mathbf{k} \\ \varepsilon_{n,\mathbf{k}} > E_{DP}}} w_{\mathbf{k}} f_{n,\mathbf{k}} (\varepsilon_{n,\mathbf{k}} - E_{DP}) \quad (2)$$

for electron donating defects like Cd_i (introducing two electron carriers), and an analogous expression for electron accepting defects like V_{Cd} (introducing two hole carriers). This sum integrates the contributions of the band energies $\varepsilon_{n,\mathbf{k}}$ with occupancies $f_{n,\mathbf{k}}$ of band n at k-point $\mathbf{k}$ and Brillouin zone weight $w_{\mathbf{k}}$. The sum runs over all occupied states above (donors) or unoccupied states below (acceptors) the E_{DP}, which represents the Fermi level of the defect-free material. After subtraction of ΔE_{bf}, ΔH_D represents the defect formation energy excluding the kinetic energy contribution resulting from the addition of carriers into the band continuum above (below) E_{DP}. Additionally, the formation energies of the charged defects Cd_i^{+2} and V_{Cd}^{-2} were calculated, where the respective carriers are removed from the supercell calculations. The potential alignment technique of Ref. 14 is used to ensure consistent energy scales between defect and host cells.

Figures 2(a) and 2(b) show the supercell size dependence of ΔH_D for the Cd_i (donor) and V_{Cd} (acceptor) defects, respectively, for supercells between 80 and 320 atoms. After subtraction of the band-filling energy ΔE_{bf}, the formation energies of the neutral defects are approximately size-independent and converge to the formation energies of the respective charged defects. These results demonstrate that defects without localized states can be described as charged defects. Since their formation energies depend explicitly on E_F, it becomes important to accurately represent the DOS of the host material, to ensure the correct mapping between the net carrier concentration, resulting from all defects and dopants, and the temperature-dependent position of the Fermi energy. In Ref. 9, this was achieved by integrating the Fermi–Dirac distribution with the DOS from quasi-particle self-consistent GW (QSGW)[15] calculations.

B. Predictions for Cd_3As_2

Considering the different merits of defects with and without localized defect states, as discussed in Sec. III A, the formation energies of the intrinsic defects were evaluated in Cd_3As_2 as a function of E_F.[9] The full defect equilibrium as a function of temperature and growth conditions is then determined by utilizing thermodynamic simulations under the condition of overall charge balance,[16] yielding the individual defect concentrations, equilibrium Fermi level, and carrier densities. The defects with delocalized charge carriers (Cd_i and V_{Cd}) tend to dominate the overall net doping, while those with localized defect states (V_{As} and anti-site defects) have higher formation energies and are much less favorable.

At the initial assumed growth temperature, the (relatively dilute) defect concentrations $c_{D,q}$ are given by an average occupation of available atomic sites with Boltzmann probability,

$$c_{D,q}\left(E_F, \{\mu\}, T\right) = N_D e^{-\Delta H_{D,q}(E_F,\{\mu\})/k_B T}, \tag{3}$$

where N_D is the site concentration, k_B is the Boltzmann constant, and $\Delta H_{D,q}(E_F, \{\mu\})$ is given by Eq. (1) above. Self-consistency is enforced by the implicit E_F dependence of the defect concentrations through $\Delta H_{D,q}$ as well as an overall charge balance between the carriers from charged defects and the free carriers that would be present at a finite growth temperature even in a defect-free material. The band-filling effects from the charged defects discussed above are accounted for by introducing a model function to mathematically describe the density of states and requiring that the model function weighted with the Fermi–Dirac distribution integrates to the net doping concentration, i.e.,

$$n_e = \int_{E_{DP}}^{\infty} \frac{g_{QSGW}(E)}{e^{(E-E_F)/k_B T} + 1} dE \tag{4}$$

for electrons and an analogous expression for holes. The model function $g_{QSGW}(E)$ for the density of states is a fit to data from QSGW calculations and serves as the best approximation to the Cd_3As_2 electronic structure. Note that for an n-doped material, Eq. (4) at zero temperature simply states that integrating the occupied density of states above the Dirac point gives the net doping (electron) concentration. Equations (1), (3), and (4) together define the self-consistent solution for competing donor/acceptor defects in equilibrium.

Figure 3 summarizes the results from thermodynamic modeling of defect equilibria at growth temperatures between 400 and 800 K in Ref. 9. For temperatures below the growth temperature, the expression for charge balance, Eq. (4), is re-evaluated to update $E_F(T)$ with fixed defect (and net doping) concentrations. In principle, the defects (e.g., Cd interstitials/vacancies) could recombine and reduce the individual defect concentrations at these lower temperatures; however, the difference between donors and acceptors remains unchanged, so the net doping and E_F are independent of any such recombinations. Under a majority of growth conditions, Cd_3As_2 favors n-type growth due to the low formation energy of Cd_i. Notably, however, the potential for neutral or p-type doping is observed for higher growth temperatures under As-rich conditions (dashed blue line in Fig. 3). This indicates an exciting possibility to tune experimental growth conditions and achieve doping-neutral Cd_3As_2.

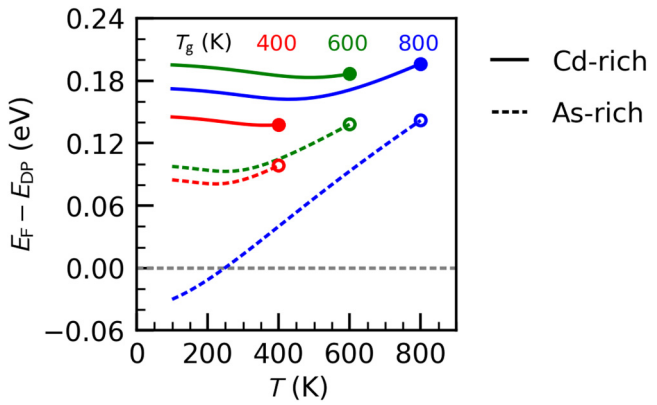

FIG. 3. Temperature dependence of the Fermi level E_F in Cd_3As_2 in the presence of defect concentrations determined for three different growth temperatures T_g (circles) in the Cd-rich (solid lines) and As-rich (dashed lines) limits.[9]

While the prospect of controlling net doping through growth is quite compelling, the behavior of $E_F(T)$ for a TSM is non-intuitive and requires careful consideration. Several features of the graph of $E_F(T)$ for both n-doped and p-doped Cd_3As_2, and even the origin of p-type doping itself, can be better understood by studying the charge balance condition, Eq. (4). The asymmetry of the DOS below/above the Dirac point and the width of the Fermi–Dirac distribution together determine the overall behavior of E_F. The effect of maintaining charge balance with varying temperatures is illustrated in Fig. 4, which graphs the Fermi–Dirac distribution [Fig. 4(a)], the QSGW model DOS (Fig. 4(b)], and the weighted areas for electrons and holes corresponding to two points on the dashed blue line of Fig. 3, i.e., 800 K [Fig. 4(c)] and 250 K [Fig. 4(d)].

At higher temperatures, the Fermi–Dirac distribution is wide enough to capture the much larger density of states below the Dirac point [see Fig. 4(b)] and introduce large numbers of hole carriers even if E_F is above the Dirac point. This means that raising the temperature requires E_F to be pushed upward to maintain charge balance, and an elevated E_F favors the formation of negatively charged acceptor-type defects (namely, the V_{Cd} in Cd_3As_2). The result of growth at this high temperature then is that acceptors can outweigh donors; so there is net p-type doping (excess holes) even though E_F is above the Dirac point [Fig. 4(c)]. Then, as the temperature is decreased, the difference between electrons and holes is maintained by lowering E_F [Fig. 4(d)], and only in the low-temperature limit does E_F move below the Dirac point.

Conversely, there is an interesting non-monotonic behavior of $E_F(T)$ in the case of n-type doping (cf. Fig. 3). This is more easily understood by starting from the low-temperature limit. At zero temperature, E_F lies above the Dirac point because of excess electrons from defects. Then, to maintain charge balance, as T increases (but is still relatively low), the positive slope of the DOS means unoccupied DOS is larger than occupied, and charge balance is maintained by decreasing E_F. Finally, once the temperature is large enough that $k_B T$ is comparable to $E_F - E_{DP}$, which depends on net doping, then the Fermi–Dirac distribution captures

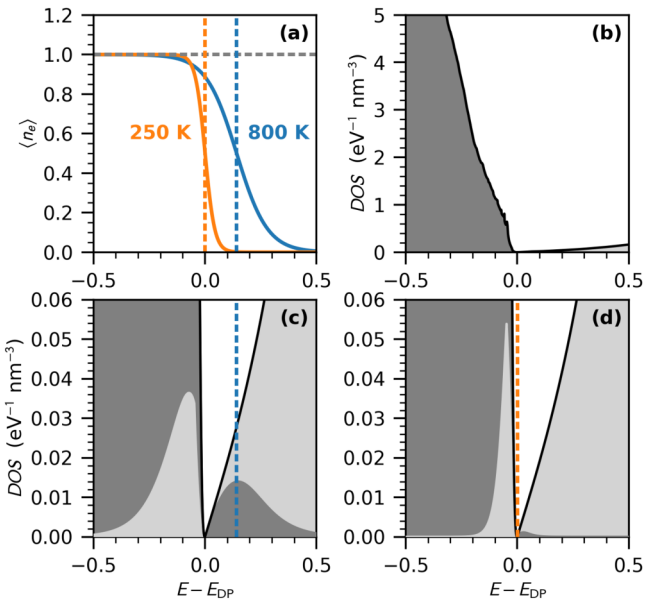

FIG. 4. (a) Fermi–Dirac occupation of electrons corresponding to As-rich growth of Cd_3As_2 at 800 K (blue) and then cooled to 250 K (orange). The temperature-dependent Fermi levels E_F are indicated by vertical dashed lines. (b) QSGW density of states data as a function of energy E near the Dirac point E_{DP}. (c) and (d) Model density of states $g_{QSGW}(E)$ weighted with the Fermi–Dirac distribution for electrons (dark gray) and holes (light gray) at the respective temperatures, 800 (c) and 250 K (d).

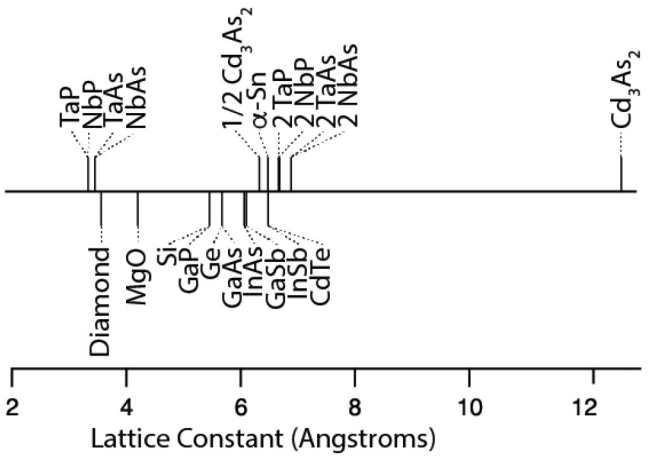

FIG. 5. Lattice constants (a = b) of TSMs with cubic or tetragonal crystal structures as well as those of typical cubic substrate materials. Values that are half (1/2) or twice (2) times the TSM lattice constant are also included in cases where they are better matched to the substrates.

the large DOS below the Dirac point and charge balance is maintained by increasing E_F.

IV. EXPERIMENTAL APPROACHES

Experiments are typically used to extract several critical pieces of information about the defects in electronic materials: which defects are present, what electronic states do they introduce, and how do they impact the electrical transport and optical properties of the material? This information, in turn, is used to guide the development of these materials and their synthesis to either mitigate or harness the effects of specific defects. Experimental techniques to probe certain aspects of defects have mainly been developed and applied in the development of semiconductors.[17–19] Many of these techniques can also be applied to topological semimetals, with some exceptions.

A. Synthesis

Synthesis can impact the defects that are formed through the selection of the growth parameters that factor into Eq. (1) (i.e., temperature and chemical potential) and influence atom incorporation into the crystal (i.e., growth rate or flux), as well as external factors such as the type of substrate that is used, if at all. Many TSMs with 3D or even 2D layered crystal structures were first synthesized as free-standing (nano)crystals through methods like chemical vapor transport, chemical vapor deposition, or solidification from a melt.[20–25] These methods typically use high temperatures and have produced crystals with some of the highest carrier mobilities.[24] However, they can sometimes produce materials that are not perfectly stoichiometric, and it may be difficult in some cases to precisely control the point defect populations.

More recently, several of these materials have been grown by epitaxial thin film methods, such as molecular beam epitaxy (MBE) and pulsed laser deposition (PLD). Examples include Cd_3As_2, Na_3Bi, and the monopnictide (Ta,Nb)(As,P) family.[26–36] Thin film synthesis can provide access to a wider window of growth conditions that are either thermodynamically or kinetically limited. The ability to vary the flux ratios of the different elements when using elemental sources (as opposed to compound sources) also allows for greater tuning of the chemical potential terms in Eq. (1), allowing the point defect population to be systematically varied.[6] However, a drawback is that TSM thin films often contain high densities of one-dimensional dislocations due to the lack of lattice-matched conventional substrates to most materials (see Fig. 5 for examples of cubic, tetragonal, and rocksalt TSMs). Careful selection of buffer layers can help to reduce the resulting dislocation densities,[27,37] but they are often much higher than those found in Si or III–V compound semiconductors.[26,27] In cases where there is even less registry of the TSM crystal structure with the underlying substrate, polycrystalline grains may also form. The characterization methods detailed below can provide insight into how these defects influence TSM properties and behavior.

B. Scanning tunneling microscopy and spectroscopy

Scanning tunneling microscopy (STM) and spectroscopy (STS) allow the arrangement and electronic structure of atoms at the surfaces of materials to be visualized based on the principle of electron tunneling between the material and a sharp probe tip.[38–40]

Since its invention, it has delivered new insight into the existence, orientation, and electronic properties of defects and impurities in semiconductors. For example, STM has been used to verify the nature of individual defects in semiconductors, including the famous EL2 arsenic antisite in GaAs,[41] and it has even been used to manipulate the positions of individual phosphorous impurities in Si for use as quantum defects.[42] STM is now delivering similar insights into the defects in TSMs. It has been used to identify the types and behavior of point defects that are present (i.e., V_{As} are donors in Cd_3As_2, V_{Na} are acceptors in Na_3Bi, and V_{Te} and intercalated Zr atoms are the prominent defects in $ZrTe_5$).[34,43,44] Because TSMs do not have a gap, understanding the location of the electronic states they introduce and their impact on the local DOS (LDOS) is also an important function of STS. Notably, this experimental technique, in conjunction with computation, has shown that many point defects in TSMs do not substantially impact the LDOS in these materials.[45,46]

Scanning tunneling microscopy has also provided important insights into the short range disorder in TSMs. Theoretical studies have long predicted that Coulomb disorder has a sizeable and nonperturbative effect on electron scattering when the Fermi level is near the Dirac point.[47] Electron and hole "puddles" form to screen the Coulomb potential around charged defects, creating an inhomogeneous distribution of carriers. While the properties of these puddles can be calculated to some degree, STS has provided more detailed information about the size and extent of the Fermi level shifts associated with these puddles,[34] which can be used to further understand their impact on magnetotransport behavior in TSMs.

Overall, STM and STS are valuable tools for directly probing point defects and charge fluctuations in TSMs. They will become increasingly useful as electrical doping and alloying are applied to design the properties of TSMs further. For example, they can be used to verify the energy levels of extrinsic dopant atoms or explore how alloying influences point defect populations. A primary challenge associated with these techniques is the extreme surface sensitivity of the technique. Measurements are often carried out on bulk crystals cleaved in vacuum.[43] It is also possible to analyze epitaxial thin films, but STM and STS require them to either be transferred from the growth to analysis chambers in ultrahigh vacuum or protected with an amorphous elemental cap (i.e., arsenic, selenium, or tellurium), which can be desorbed in vacuum prior to measurements. It is also important to emphasize that theoretical computations must be used to interpret the experimental data.

As additional TSM materials are investigated, STM/STS is poised to be a valuable tool in determining the types of point defects that are most prevalent and the degree to which they introduce potential variations. Linking them to synthesis conditions and electrical transport behavior will further support efforts to understand how defects with states in the bands influence the Fermi level and fermion scattering and how to manipulate them.

C. Electron microscopy

The presence and properties of extended defects are best evaluated by electron microscopy. One-dimensional dislocations and two-dimensional defects, such as twins, stacking faults, and grain boundaries, can be found in bulk crystals.[48] Characterization of the types of extended defects is the first important step in understanding their role in the behavior of TSMs. Grain statistics in polycrystalline materials can be determined through electron backscatter diffraction (EBSD), while threading dislocation densities have similarly been quantified using electron channeling contrast imaging (ECCI).[27,49] Both methods are available on scanning electron microscopes and allow for larger area analysis (100 s of μm^2) with minimal sample preparation. Transmission electron microscopy (TEM) offers a closer inspection of the details of extended defects. For example, it has been revealed that TaAs and TaP monopnictide bulk crystals often contain high concentrations of stacking faults that cause the materials to become nonstoichiometric.[48] Electron microscopy has also revealed that misalignment of these stacking faults during thin film epitaxy leads to the appearance of domain boundaries as 3D nucleated islands join together.[30,36] Electron microscopy has likewise been invaluable in verifying that a reduction of dislocations in Cd_3As_2 through annihilation in thicker buffer layers results in higher electron mobilities.[37]

Studying extended defects in TSMs is important for several reasons. First, it aids in the quest to understand structure-property relationships. One example is the influence of extended defects on electron scattering. The nature of TSM states protects against electron and hole backscattering but allows for scattering in other directions. Determining the extent to which dislocations and grain boundaries affect electron mobility, especially with respect to their strong influence in semiconductors, requires extensive knowledge of the defects that are in the material. Second, this knowledge is also important for linking defect formation with synthesis conditions so that defect formation can be avoided in the first place. Thin film growth on lattice-mismatched substrates can lead to 3D island nucleation and the formation of dislocations, twins, stacking faults, and other extended defects. For example, during early efforts to grow Cd_3As_2 on III-V semiconductor substrates, it was determined that twin defects were forming at high densities, leading to poor electron mobility. Switching to a miscut substrate suppressed the formation of these defects and improved transport performance.[26] Fortunately, insights and approaches for controlling semiconductor synthesis, learned over decades, can also be applied to TSM thin film epitaxy.

D. Magnetotransport

Studying the behavior of carrier transport under the application of electric and magnetic fields is the most common and accessible method for studying the defects in TSMs. Here, defects are not imaged or detected directly, but their impact on the Fermi level, carrier mobility, and scattering behavior can provide valuable information about their charge states and the potential energy landscapes they create. These measurements can also provide information about how the presence of defects impacts phenomena that are typically observed in TSMs.

As in the case of semiconductors, the Hall effect serves as a suitable starting point for obtaining net carrier concentrations and mobilities. In single band systems, Hall resistivity measurements at low magnetic field determine the carrier concentration. In conjunction with the measurements of longitudinal resistivity, mobility can be calculated. In the absence of extrinsic dopants, carrier

concentrations are often dictated by the native defect populations. Measuring the net carrier concentration can, therefore, provide insight into which ones dominate.[6] Point and extended defects can scatter carriers, leading to lower mobility. The ability to systematically vary specific types of defects through control of the synthesis conditions may then offer indirect information about their scattering behavior. For example, lowering the threading dislocation density in Cd_3As_2 epitaxial thin films significantly improves electron mobility, suggesting that they act as strong scattering sources.[37] However, altering the balance of cadmium vacancy and interstitial concentrations in the same material does not appear to substantially influence the electron mobility, suggesting that they do not influence scattering to the same extent as dislocations.[6] One important aspect to note is that interpretation of Hall effect measurements may be straightforward in Dirac semimetals in which the band touching nodes degenerate and are located well away from any trivial bands. This is the case for Cd_3As_2. However, sets of band touching nodes may be located at different energies in some Weyl semimetals, causing the Fermi level to cross them at different locations. Additionally, trivial bands may also be located near the Fermi level in many TSMs, resulting in the coexistence of multiple electron-like and hole-like Fermi surfaces. These aspects complicate the interpretation of magnetotransport measurements.

High field magnetoresistance (MR) measurements can help us to uncover the presence of multiple types of charge carriers. Generally, MR occurs when an applied transverse magnetic field alters the carrier trajectories resulting in a change in the measured resistance. Semiclassical MR can be thought to originate from the Lorentz force acting on carriers moving transverse to the current direction. Disorder scattering can alter this semiclassical MR—changing its magnitude and scaling as a function of the magnetic field. Given the possibility of extracting quantitative information about scattering centers (including defects), we spend some time here detailing semiclassical MR and MR in the presence of disorder in TSMs.

In the event of multiple bands crossing the Fermi energy, we can write the total longitudinal and Hall conductivities by summing contributions from each band,

$$\sigma_{xx}(H) = \sum_{i=1,..,n} \frac{|n_i| e\mu_i}{1 + (\mu_i H)^2},$$

$$\sigma_{xy}(H) = \sum_{i=1,..,n} \frac{n_i e\mu_i^2 H}{1 + (\mu_i H)^2},$$

where n_i and μ_i are the carrier density and mobility of carriers for the ith band and H is the applied magnetic field. This is the so-called multi-band model, and its simplified form is broadly useful in the basic analysis of magnetotransport data. In semimetallic systems, these equations are often restricted to two bands. In this special case, the longitudinal and Hall resistivities can be expressed simply as follows:

$$\rho_{xx}(H) = \frac{1}{e} \frac{(n_h\mu_h + n_e\mu_e) + (n_h\mu_e + n_e\mu_h)\mu_h\mu_e H^2}{(n_h\mu_h + n_e\mu_e)^2 + (n_h - n_e)^2\mu_h^2\mu_e^2 H^2},$$

$$\rho_{xy}(H) = -\frac{H}{e} \frac{(n_h\mu_h^2 - n_e\mu_e^2) + (n_h\mu_e - n_e\mu_h)\mu_h^2\mu_e^2 H^2}{(n_h\mu_h + n_e\mu_e)^2 + (n_h - n_e)^2\mu_h^2\mu_e^2 H^2},$$

where the subscript denotes electron-like or hole-like carriers and the carrier densities are positive. The MR scales quadratically with the magnetic field. It should also be noted that ρ_{xx} will saturate at a magnetic field that scales with the difference between the electron and hole populations and will become non-saturating in the case of perfect compensation ($n_e = n_h$). The magnitude of the MR increases with increasing carrier mobilities. Figures 6(a) and 6(c) schematically summarize the longitudinal resistivity and the tangent of the Hall angle in a simple, nearly compensated two-band model.

In many uncompensated semimetals, high carrier mobilities originating from linear bands paired with a disorder can result in a different dominant MR mechanism. The presence of charged, screened disorder sites generates a smooth potential landscape. The motion of carriers in an applied magnetic field can be described as the sum of fast cyclotron motion and a slower diffusion of the guiding center. At low fields, when the cyclotron radius of the carrier is large, its trajectory is not significantly affected by the potential landscape. The MR in this low field range exhibits a quadratic behavior, similar to compensated semimetals. When the cyclotron radius is reduced below the average distance between scattering centers, its trajectory is altered by the disorder potential landscape, leading to increased resistance

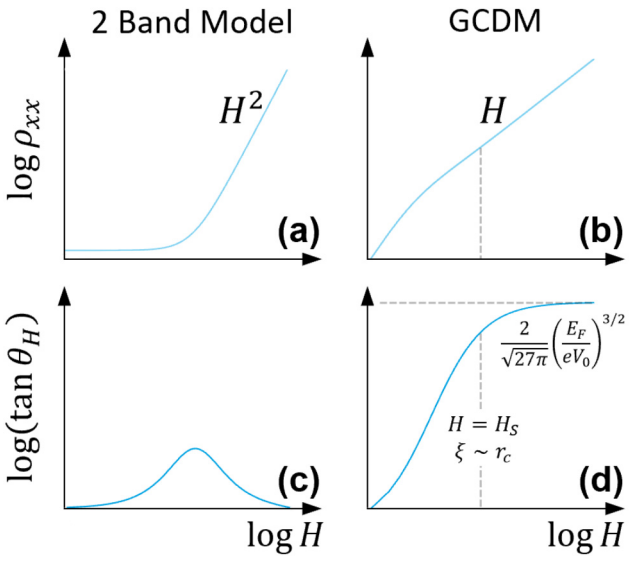

FIG. 6. Schematic logarithmic dependence of (a) and (b) $\rho_{xx}(H)$ and (c) and (d) $\tan\theta_H \equiv \rho_{xy}/\rho_{xx}$ for a nearly compensated two-band model [right: (a) and (c)] and the guiding center diffusion model [left: (b) and (d)]. The two-band model can generate nonsaturating quadratic MR paired with a $\tan\theta_H$ that peaks and decreases while the MR continues to increase. At even larger fields, the MR from compensation always saturates, leading to $\tan\theta_H \sim H$. Meanwhile, the MR stemming from the GCDM for a single carrier is superlinear at low fields, becoming linear above $H = H_S$. Linear MR paired with a linear, single-carrier Hall effect leads to saturating $\tan\theta_H$ as a function of the field.

with a linear dependence on the magnetic field. This behavior is captured by the Guiding Center Diffusion Model (GCDM), from which the disorder potential (eV_0) and the disorder length scale (ξ) can be determined.[50,51] The magnetic field at which the MR behavior transitions from quadratic to linear, H_S, is linked to the average distance of scattering centers, ξ, through the relationship

$$\xi = \frac{m_e^* v_F}{e\mu_0 H_S}.$$

Concurrently with the linear MR (LMR), the tangent of the Hall angle saturates to a constant value as a function of the field. H_S can be determined from the value at which the tangent of the Hall angle saturates,

$$\tan\theta_H = \frac{\rho_{xy}}{\rho_{xx}} = A\tanh\left(\frac{H}{H_S}\right).$$

The tangent of the Hall angle value is also related to the strength of the disorder potential through the relationship

$$\tan\theta_H|_{H>H_S} = \frac{2}{\sqrt{27\pi}}\left(\frac{E_F}{eV_0}\right)^{3/2},$$

where E_F is the Fermi energy. An important caveat is that the GCDM mechanism only applies to scattering by smoothly varying potentials. This situation is valid for charged centers that are screened by the large dielectric constants found in many TSMs.[43,47,50,51] To date, the GCDM model has yielded information about the point defect scattering centers in TaP, NbP, and Cd_3As_2, where disorder potentials are of the order of 20–60 meV.[6,51] Figures 6(b) and 6(d) show the longitudinal resistivity and the tangent of the Hall angle arising in the GCDM. Unlike the two-band model, $\tan\theta_H$ as a function of the field saturates to a value dependent on the Fermi energy and the disorder potential strength.

Quantitative information about the carrier properties and scattering can also be obtained from Shubnikov–de Haas (SdH) oscillations that often occur on top of the baseline MR. These quantum oscillations occur when the cyclotron motion of charged carriers in the plane normal to the magnetic field direction is quantized by Landau level splitting under high applied magnetic fields. The magnitude of the MR oscillates as the Landau levels cross the Fermi energy. The oscillatory component of the MR can be fit with the Lifshitz–Kosevich model,

$$\frac{\Delta R_{xx}}{R_{xx}} = \left(\frac{\hbar\omega_c}{2E_F}\right)^{\frac{1}{2}}\frac{\lambda}{\sinh\lambda}e^{-\lambda_D}\cos\left(\frac{\hbar\pi k_F^2}{eH}+\phi\right),$$

where $\omega_c = \frac{eH}{m_c}$ is the cyclotron frequency, m_c is the cyclotron mass, $\lambda = \frac{2\pi^2 k_B T}{\hbar\omega_c}$, and $\lambda_D = \frac{2\pi^2 k_B T_D}{\hbar\omega_c}$. $T_D = \frac{\hbar}{2\pi k_B \tau_Q}$ is the Dingle temperature, and τ_Q is the quantum lifetime. Thus, SdH oscillation fitting is practical for extracting E_F, m_c, and τ_Q, which is also associated with scattering from potential fluctuations and other disorders.[24]

V. CURRENT UNDERSTANDING OF ROLE OF DEFECTS

As in semiconductors, defects have the most potential to influence fermion transport in TSMs. However, the scattering mechanisms may vary in nuanced ways due to the slightly different behavior of defects in these systems. For example, the absence of a bandgap and screening of charged defects result in smooth, long-range potential variations without the introduction of conventional bound states. This situation will alter the dominant scattering mechanisms and impact the MR behavior. The role of defects on the electronic structure has also been the subject of theoretical investigation. Dirac and Weyl nodes were originally thought to be unperturbed by the types of weak disorder introduced by defects.[52,53] Yet, more recent studies have questioned this picture, suggesting instead that the presence of nonzero disorder introduces finite density of states at the nodes.[54–56] It is unclear if or how point and extended defects introduce strong enough potential variations to influence the electronic structure at the nodes substantially.

Elucidating the details of how defects influence the properties and behaviors of TSMs will require deliberate control of specific defect types as well as the overall Fermi level to start to probe transport behavior near the Dirac and Weyl nodes. Epitaxial thin film synthesis can provide a route to point defect control via access to a wide range of crystal growth conditions (i.e., temperature, flux ratios, and growth rate). Measurements, particularly those that can determine local energy potential variations introduced by defects, such as STM/STS and magnetotransport, are of particular value in filling in knowledge gaps around the types of states they may introduce into the electronic structure (if any) and their role in fermion scattering. Experimental findings must also be correlated with theoretical computations and predictions to understand the link between measured parameters (i.e., magnetoresistance, optical absorption) and the physical way in which defects influence them. Here, we add more commentary on the three aspects of defects that play an important role in the eventual use of TSMs in applications.

A. Impact on Fermi level

At low temperatures and in the absence of extrinsic dopants, point defects are the main source of free carriers. Interestingly, bulk and thin film synthesized forms of the same material can have very different carrier concentrations and Fermi levels. For example, bulk crystals of Cd_3As_2 are typically n-type, with electron concentrations in the 10^{18} cm^{-3} range, while the electron concentration in epitaxial Cd_3As_2 thin film layers is often found to be lower by one to two orders of magnitude.[24,33,37,43,57] Density functional theory calculations have provided insight into the role of temperature and chemical potential on the ability to shift the balance of donor and acceptor defects.[9] The greater range of synthesis conditions that are available in thin film synthesis can enable a larger range of carrier concentrations (10^{16}–10^{18} cm^{-3}) and Fermi levels to be reached. Cd_3As_2 appears to be a relatively well-behaved material in this regard. Conversely, monopnictides exhibit very different doping characteristics. Again, bulk crystals exhibit moderate electron doping (10^{18} cm^{-3}), but the limited number of monopnictide epitaxial thin films that have been grown so far all exhibit exceedingly high hole concentrations (10^{20}–10^{21} cm^{-3}),[28,30,36,58] except for one instance of NbAs, which showed high electron concentrations

(10^{21}–10^{22} cm^{-3}).[29] Adjusting the synthesis conditions does not substantially shift this concentration.[30] Deriving the same insights into defect control from DFT will be important for being able to shift the Fermi level in epitaxial thin films of monopnictides into ranges that are appropriate for device applications. Broader insights into which TSMs will offer greater tunability of point defects will be important for selecting which TSMs are best suited for devices, as well as to shift the Fermi level toward the Dirac and Weyl nodes to enable new scientific investigations into the basic properties of TSMs.

Extrinsic doping has proven to be the most effective approach for controlling the Fermi level in semiconductors, and limited efforts to extrinsically dope TSMs have so far worked as well.[57] Cd_3As_2 has been a good test case, where Se and Te have been used to increase the electron concentration. At relatively low concentrations (<atomic percent), these charged dopant impurities do not substantially affect electron mobility or the electronic structure. It should be noted that extrinsic electron doping of Cd_3As_2, which is already intrinsically n-type, could be reasonably expected. Extrinsically doping it p-type may prove to be more challenging, and DFT calculations will be indispensable in selecting proper p-type dopants. However, achieving both p- and n-type extrinsic doping in TSMs will create new possibilities for designing them for specific applications as well as studying the electronic structure and transport behavior near the band touching nodes.

B. Impact on carrier transport

Another difference between bulk and thin film TSMs is the mobilities that can be reached. Cd_3As_2 is the most extensively studied in this respect. While bulk crystals have exhibited electron mobilities up to 10^7 $cm^2/V\,s$, thin films have reached mobility ceilings of 40 000 $cm^2/V\,s$.[24,37] Dislocations are more prevalent in thin films and are known to lower electron mobility.[27,37] However, our current understanding of the strength by which they scatter electrons does not fully account for the two-to-three order of magnitude difference in values. More information is needed to understand how defects, disorder, or other aspects of thin films may affect mobility.

On the other hand, a more detailed picture is beginning to emerge about how point defects influence MR behavior. Non-saturating linear MR (LMR) is commonly observed in TSMs, and its origin has been explained by several different mechanisms tied to disorders.[59–61] The role of defects was not explicitly explored until recently, when it became possible to tie defect populations to the magnitude of LMR using the equations and the GCDM model presented in Sec. IV D.[6,51] In particular, the ability to systematically vary defect populations by carefully adjusting the flux ratios during thin film growth provided a way to quantitatively test the GCDM model and verify its validity.[6] In this framework, the smoothly varying potentials introduced by charged point defects, even when they do not substantially alter the density of states, has a profound influence on the LMR magnitude. A main takeaway from this picture is that point defects can play a role in tuning the LMR, but high overall mobility is required to achieve large LMR values. Analysis within the GCDM framework also provides a method for probing the extent of defect-related disorder in TSM crystals.

C. Surface defects

Much of the discussion above, with the notable exception of the STM measurement section, has focused on point and extended defects in the TSM bulk. Defects at surfaces (and interfaces) also play a role in TSM electronic and transport properties, particularly if a larger proportion of current flows through surface states. This is certainly the case in quantum confined TSM thin films, where a gap opens in the bulk states. Their behavior must also be understood as TSMs are designed for specific applications that rely on the properties of those surface states, including TSMs for ultrathin interconnects and catalysis.

Surface defect formation is influenced by several factors. They include their formation energies, the dynamics involved in cleaving bulk crystals, and the thermodynamics and kinetics of adatom incorporation and surface reconstruction involved in bulk crystal and thin film growth. Post growth, oxidation of surfaces presents an additional route for defect formation. Cd_3As_2 surfaces are known to oxidize. A computational study of Cd_3As_2 indicates that the mechanisms of oxide formation depend on some degree of the surface termination of the Cd_3As_2 surface but that oxidation of the Cd_3As_2 (112) surface does not significantly impact the electronic structure of the surface states.[62] These results were validated by XPS measurements. However, it is not yet clear whether the robustness of the surface electronic structure holds up to oxidation in other materials.

Surface defects have also been found to enhance the catalytic behavior of TSMs for the hydrogen evolution reaction.[63] Defects and dangling bonds provide a rich environment in which reactants, intermediaries, and products can bind to the TSM surface and interact with electrons in the crystal. Oxidation can change the balance of those sites, ultimately affecting the catalytic performance.

Interestingly, steps can be taken to passivate the surface defects. Galletti *et al.* found that in Cd_3As_2, surface passivation with nitrogen plasma treatment helped to improve low-temperature carrier mobilities and lower the longitudinal resistivities, especially in very thin films (<25 nm).[64] The plasma treatment was correlated with a measured reduction in strongly electronegative OH- species adsorbed at dangling bond sites. It is presumed that these OH- species influence carrier scattering as well as promote low-mobility hole conduction, in addition to high mobility electron conduction. Nitrogen passivation of the dangling bond sites blocks OH- adsorption and enhances n-type conduction through the surface states.

The impact of surface defects on electrical transport behavior has also been theoretically and experimentally explored in a handful of materials. Computational studies of several Weyl TSM materials (including CoSi, TaAs, and NbAs) in the absence of defects suggest that Fermi arc states can support unconventional resistivity scaling, where the resistance area (RA) product decreases as the cross-sectional area decreases.[35,65] This is in contrast to conventional metals, like Cu, where the RA product increases due to increased electron scattering by surface states. However, the presence of surface defects may cause resistivity to revert back to conventional scaling laws, depending on the concentration of defects, the film thickness, and the details of the material and its Fermi arc

states. This behavior may have interesting implications for the use of TSMs as interconnects in integrated circuits. Focused experimental investigation will be critical for validating these theoretical findings and understanding the impact of surface defects on carrier transport.

VI. SUMMARY AND OPEN QUESTIONS

Defects play an important role in the properties and behavior of TSMs. Building on our knowledge of defects in semiconductors, we already have useful frameworks for conceptualizing and probing certain aspects of defects, but we are still starting to understand the nuanced differences in mechanisms and the extent of their impact on TSMs specifically. Filling these knowledge gaps will require focused research efforts and improved capabilities in the following areas:

- Appropriate substrates and/or buffer structures are needed to minimize the formation of dislocations and other extended defects in order to realize TSM thin films with high carrier mobilities. Further control of specific extended defect types (i.e., dislocations, stacking faults, grain boundaries) as well as experimental measurement of the potential variations they introduce will also be helpful in determining the extent to which they reduce carrier mobilities. Overall, this information will serve as design guidelines for how much or little attention should be devoted to reducing them.
- Fermi level tunability via control of native point defects and extrinsic doping is important for designing TSMs for device applications as well as fundamental science investigations. Detailed computational evaluation of native point defect formation as a function of synthesis conditions (i.e., temperature and chemical potential) is needed for most TSMs to guide synthesis efforts. Enhancing the flexibility of synthesis methods to suppress point defect formation is also needed to practically achieve low concentrations of unintentional carriers (a particular problem for thin film monopnictides). Similarly, greater insight into which impurities may serve as effective n- or p-type dopants will aid in the development of TSMs for devices.
- More broadly, understanding how defects and impurities with localized and delocalized characters impact carrier transport and the electronic structure near the Dirac and Weyl nodes will give us more insight into the TSM design for applications.

ACKNOWLEDGMENTS

This work was funded by the U.S. Department of Energy (DOE), Office of Science (SC), Basic Energy Sciences, Physical Behavior of Materials program as part of the "Disorder in Topological Semimetals" project. The Alliance for Sustainable Energy, LLC, operates the National Renewable Energy Laboratory (NREL) under contract DE-AC36-08GO28308. The views expressed in the article do not necessarily represent the views of DOE or the U.S. Government.The US government retains and the publisher, by accepting the article for publication, acknowledges that the US government retains a nonexclusive, paid-up, irrevocable, worldwide license to publish or reproduce the published form of this work, or allow others to do so, for US government purposes.

AUTHOR DECLARATIONS

Conflict of Interest

The authors have no conflicts to disclose.

Author Contributions

Kirstin Alberi: Conceptualization (lead); Funding acquisition (lead); Project administration (lead); Resources (lead); Writing – original draft (equal); Writing – review & editing (equal). **Chase Brooks:** Writing – original draft (equal); Writing – review & editing (equal). **Ian Leahy:** Writing – original draft (equal); Writing – review & editing (equal). **Stephan Lany:** Conceptualization (supporting); Writing – original draft (equal); Writing – review & editing (equal).

DATA AVAILABILITY

The data that support the findings of this study are available from the corresponding author upon reasonable request.

REFERENCES

[1]D. N. Basov, R. D. Averitt, and D. Hsieh, "Towards properties on demand in quantum materials," Nat. Mater. **16**, 1077 (2017).
[2]B. Keimer and J. E. Moore, "The physics of quantum materials," Nat. Phys. **13**, 1045 (2017).
[3]L. M. Schoop, F. Pielhofer, and B. V. Lotsch, "Chemical principles of topological semimetals," Chem. Mater. **30**, 3155–3176 (2018).
[4]A. A. Burkov, "Topological semimetals," Nat. Mater. **15**, 1145 (2016).
[5]M. Z. Hasan, G. Chang, I. Belopolski, G. Bian, S.-Y. Xu, and J.-X. Yin, "Weyl, Dirac and high-fold chiral fermions in topological quantum matter," Nat. Rev. Mater. **6**, 784 (2021).
[6]J. N. Nelson, I. A. Leahy, A. D. Rice, C. Brooks, G. Teeter, M. van Schilfgaarde, S. Lany, B. Fluegel, M. Lee, and K. Alberi, "Direct link between disorder and magnetoresistance in topological semimetals," Phys. Rev. B **107**, L220206 (2023).
[7]S. Lany and A. Zunger, "Assessment of correction methods for the band-gap problem and for finite-size effects in supercell defect calculations: Case studies for ZnO and GaAs," Phys. Rev. B **78**, 235104 (2008).
[8]C. Freysoldt, B. Grabowski, T. Hickel, J. Neugebauer, G. Kresse, A. Janotti, and C. G. Van de Walle, "First-principles calculations for point defects in solids," Rev. Mod. Phys. **86**, 253 (2014).
[9]C. Brooks, M. van Schilfgaarde, D. Pashov, J. N. Nelson, K. Alberi, D. S. Dessau, and S. Lany, "Band energy dependence of defect formation in the topological semimetal Cd_3As_2," Phys. Rev. B **107**, 224110 (2023).
[10]S. Lany and A. Zunger, "Anion vacancies as a source of persistent photoconductivity in II-VI and chalcopyrite semiconductors," Phys. Rev. B **72**, 035215 (2005).
[11]H. Wang and A.-B. Chen, "Calculation of shallow donor levels in GaN," J. Appl. Phys. **87**, 7859–7863 (2000).
[12]S. Zhang and J. E. Northrup, "Chemical potential dependence of defect formation energies in GaAs: Application to Ga self-diffusion," Phys. Rev. Lett. **67**, 2339 (1991).
[13]C. Persson, Y.-J. Zhao, S. Lany, and A. Zunger, "*n*-type doping of $CuInSe_2$ and $CuGaSe_2$," Phys. Rev. B **72**, 035211 (2005).
[14]S. Lany and A. Zunger, "Accurate prediction of defect properties in density functional supercell calculations," Modell. Simul. Mater. Sci. Eng. **17**, 084002 (2009).

[15]D. Pashov, S. Acharya, W. R. Lambrecht, J. Jackson, K. D. Belashchenko, A. Chantis, F. Jamet, and M. van Schilfgaarde, "Questaal: A package of electronic structure methods based on the linear muffin-tin orbital technique," Comput. Phys. Commun. **249**, 107065 (2020).
[16]S. Lany, Y.-J. Zhao, C. Persson, and A. Zunger, "Halogen *n*-type doping of chalcopyrite semiconductors," Appl. Phys. Lett. **86**, 042109 (2005).
[17]H. J. Queisser and E. E. Haller, "Defects in semiconductors: Some fatal, some vital," Science **281**, 945–950 (1998).
[18]A. Alkauskas, M. D. McCluskey, and C. G. Van De Walle, "Tutorial: Defects in semiconductors—Combining experiment and theory," J. Appl. Phys. **119**, 1811001 (2016).
[19]J. M. Deen and F. Pascal, "Electrical characterization of semiconductor materials devices—Review," J. Mater. Sci.: Mater. Electron. **17**, 549–575 (2006).
[20]S.-Y. Xu, I. Beloposlki, N. Alidoust, M. Neupane, G. Bian, C. Zhang, R. Sankar, G. Chang, Z. Yuan, C.-C. Lee, S.-M. Huang, H. Zheng, J. Ma, D. S. Sanchez, B. Wang, A. Bansil, F. Chou, P. P. Shibayev, H. Lin, S. Jia, and M. Z. Hasan, "Discovery of a Weyl Fermion semimetal and topological Fermi arcs," Science **349**, 613 (2015).
[21]Z. Liu, B. Zhou, Y. Zhang, Z. Wang, H. Meng, D. Prabhakaran, S.-K. Mo, Z. Shen, Z. Fang, X. Dai, Z. Hussain, and Y. Chen, "Discovery of a three-dimensionaltopological Dirac semimetal, Na_3Bi," Science **343**, 864 (2014).
[22]Z. Liu, J. Jiang, B. Zhou, Z. Wang, Y. Zhang, H. Meng, D. Prabhakaran, S.-K. Mo, H. Peng, P. Dudin, T. Kim, Z. Fang, X. Dai, Z. Shen, Z. Hussain, and Y. Chen, "A stable three-dimensional topological Dirac semimetal Cd_3As_2," Nat. Mater. **13**, 677 (2014).
[23]C. Shekhar, A. K. Nayak, Y. Sun, M. Schmidt, M. Nicklas, I. Leermakers, U. Zeitler, Y. Skourski, Z. Wosnitza, Y. Chen, W. Schnelle, H. Borrmann, Y. Grin, C. Felser, and B. Yan, "Extremely large magnetoresistance and ultrahigh mobility in the topological Weyl semimetal candidate NbP," Nat. Phys. **11**, 645 (2015).
[24]T. Liang, Q. Gibson, M. N. Ali, M. Liu, R. Cava, and N. Ong, "Ultrahigh mobility and giant magnetoresistance in the Dirac semimetal Cd_3As_2," Nat. Mater. **14**, 280–284 (2016).
[25]S. Hao, J. Zeng, T. Xu, X. Cong, C. Wang, C. Wu, Y. Wang, X. Liu, T. Cao, G. Su, L. Jia, Z. Wu, Q. Lin, L. Zhang, S. Yan, M. Guo, Z. Wang, P. Tan, L. Sun, Z. Ni, S.-J. Liang, X. Cui, and F. Miao, "Low-temperature eutectic synthesis of $PtTe_2$ with weak antilocalization and controlled layer thinning," Adv. Funct. Mater. **28**, 1803746 (2018).
[26]T. Schumann, M. Goyal, H. Kim, and S. Stemmer, "Molecular beam epitaxy of Cd_3As_2 on a III-V substrate," APL Mater. **4**, 126110 (2016).
[27]A. Rice, K. Park, E. Hughes, K. Mukherjee, and K. Alberi, "Defects in Cd_3As_2 epilayers via molecular beam epitaxy and strategies for reducing them," Phys. Rev. Mater. **3**, 121201(R) (2019).
[28]W. Yanez, Y. Ou, R. Xiao, S. Ghosh, J. Dwivedi, E. Steinbronn, A. Richardella, K. A. Mkjhoyen, and N. Samarth, "Giant dampinglike-torque efficiency in naturally oxidized polycrystalline TaAs thin films," Phys. Rev. Appl. **18**, 054004 (2022).
[29]W. Yanez-Parreno, Y.-S. Huang, S. Ghosh, S. Islam, J. E. Gomez, E. Steinebronn, A. Richardella, L. Aviles-Felix, A. Butera, K. A. Mkhoyan, and N. Samarth, "Thin film growth of the Weyl semimetal NbAs," Phys. Rev. Mater. **8**, 034204 (2024).
[30]J. N. Nelson, A. D. Rice, R. Kurleto, A. Shackelford, Z. Sierzega, P. Hao, B. S. Berggren, C.-S. Jiang, A. G. Norman, M. E. Holtz, J. S. Mangum, I. A. Leahy, K. N. Heinselman, H. Ness, M. van Schilfgaarde, D. S. Dessau, and K. Alberi, "Thin film TaAs: Developing a platform for Weyl semimetal devices," Matter **6**, 1–14 (2023).
[31]A. Bedoya-Pinto, A. K. Pandeya, D. Liu, H. Deniz, K. Chang, H. Tan, H. Han, J. Jena, I. Kostanovskiy, and S. S. Parkin, "Realization of epitaxial NbP and TaP Weyl semimetal thin films," ACS Nano **14**, 4405 (2020).
[32]Y. Nakazawa, M. Uchida, S. Nishihaya, M. Kreiner, Y. Kozuka, Y. Taguchi, and M. Kawasaki, "Structural characterisation of high-mobility Cd_3As_2 films crystallised on $SrTiO_3$," Sci. Rep. **8**, 2244 (2018).
[33]K. Nakazawa, M. Uchida, S. Nishihaya, S. Sato, J. Matsuno, and M. Kawasaki, "Molecular beam epitaxy of three-dimensionally thick Dirac semimetal Cd_3As_2 films," APL Mater. **7**, 071109 (2019).
[34]M. T. Edmonds, J. L. Collings, J. Hellerstedt, I. Yudhistra, L. C. Gomes, J. N. Rodrigues, S. Adam, and M. S. Fuhrer, "Spatial charge inhomogeneity and defect states in topological Dirac semimetal thin films Na_3Bi," Sci. Adv. **3**, eaao6661 (2017).
[35]S.-W. Lien, I. Garate, U. Bajpai, C.-Y. Huang, C.-H. Hsu, N. A. Lanzillo, A. Bansil, T.-R. Chang, G. Liang, H. Lin, and C.-T. Chen, "Unconventional resistivity scaling in topological semimetal CoSi," npj Quantum Mater. **8**, 3 (2023).
[36]J. Sadowski, J. Z. Domagala, W. Zajkowska, S. Kret, B. Seredynski, M. Gryglas-Borysiewicz, Z. Ogorzalek, R. Bozek, and W. Pacuski, "Structural properties of TaAs Weyl semimetal thin films grown by molecular beam epitaxy on GaAs(001) substrates," Cryst. Growth Des. **22**, 6039–6045 (2022).
[37]M. Goyal, S. Salmani-Rezaie, T. N. Pardue, B. Guo, D. A. Kealhofer, and S. Stemmer, "Carrier mobilities of (001) cadmium arsenide films," APL Mater. **8**, 051106 (2020).
[38]R. Feenstra, "Cross-sectional scanning tunneling microscopy of III-V semiconductor structures," Semicond. Sci. Technol. **9**, 2157 (1994).
[39]J. Kubby and J. Boland, "Scanning tunneling microscopy of semiconductor surfaces," Surf. Sci. Rep. **26**, 61 (1996).
[40]Q.-K. Xue, T. Hashizume, and T. Sakurai, "Scanning tunneling microscopy of III-V compound semiconductor (001) surfaces," Prog. Surf. Sci. **56**, 1–131 (1997).
[41]R. Feenstra, J. Woodall, and G. Pettit, "Observation of bulk defects by scanning tunneling microscopy and spectroscopy: Arsenic antisite defects in GaAs," Phys. Rev. Lett. **71**, 1176 (1993).
[42]S. Schofield, N. Curson, M. Simmons, F. Ruess, T. Hallam, L. Overbeck, and R. Clark, "Atomically precise placement of single dopants in Si," Phys. Rev. Lett. **91**, 136104 (2003).
[43]S. Jeon, B. B. Zhou, A. Gyenis, B. E. Feldman, I. Kimchi, A. C. Potter, Q. D. Gibson, R. J. Cava, A. Vishwanath, and A. Yazdani, "Landau quantization and quasiparticle interference in the three-dimensional Dirac semimetal Cd_3As_2," Nat. Mater. **13**, 851 (2014).
[44]B. Salzmann, A. Pulkkinen, B. Hildebrand, T. Jaouen, S. Zhang, E. Martino, Q. Li, G. Gu, H. Berger, O. Yazyev, A. Akrap, and C. Monney, "Nature of native atomic defects in $ZrTe_5$ and their impact on the low-energy electronic structure," Phys. Rev. Mater. **4**, 114201 (2020).
[45]W.-X. Wang, K. Li, X. Dong, H. Xie, C. Xu, K. Liu, J. Song, Y. Liu, K.-K. Bai, Y.-W. Wei, and X. Xu, "Visualizing the atomic defects by scanning tunneling microscopy in the type-II Dirac semimetal $NiTe_2$," Phys. Scr. **98**, 015020 (2023).
[46]P. C. Aguilar, F. Calleja, C.-N. Kuo, B. Ghosh, A. Agarwal, A. Politano, A. L. Vazquez de Pargo, R. Miranda, J. A. Silva-Guillen, and M. Garnica, "Atomic-scale study of type-II Dirac semimetal $PtTe_2$ surface," J. Phys.: Mater. **5**, 044003 (2022).
[47]B. Skinner, "Coulomb disorder in three-dimensional Dirac systems," Phys. Rev. B **90**, 060202(R) (2014).
[48]T. Besara, D. Rhodes, K.-W. Chen, S. Das, Q. Zhang, J. Sun, B. Zeng, Y. Xin, L. Balicas, R. Baumbach, E. Manousaki, D. Singh, and T. Siegrist, "Coexistence of Weyl physics and planar defects in the semimetals TaP and TaAs," Phys. Rev. B **93**, 245152 (2016).
[49]Y. Picard, M. Liu, J. Lammatao, R. Kamaladasa, and M. De Graef, "Theory of dynamical electron channeling contrast images of near-surface crystal defects," Ultramicroscopy **146**, 71–78 (2014).
[50]J. C. Song, G. Refael, and P. A. Lee, "Linear magnetoresistance in metals: Guiding center diffusion in a smooth random potential," Phys. Rev. B **92**, 180204(R) (2015).
[51]I. A. Leahy, Y.-P. Lin, P. E. Siegfrie, A. C. Treglia, J. C. Song, R. M. Nandkishore, and M. Lee, "Nonsaturating large magnetoresistance in semimetals," Proc. Natl. Acad. Sci. U.S.A. **115**, 10570–10575 (2018).
[52]B. Sbierski, G. Pohl, E. J. Bergholtz, and P. W. Brouwer, "Quantum transport of disordered Weyl semimetals at the nodal point," Phys. Rev. Lett. **113**, 026602 (2014).
[53]B. Roy and S. Das Sarma, "Diffusive quantum criticality in three-dimensional disordered Dirac semimetals," Phys. Rev. B **90**, 241112(R) (2014).

[54]R. Nandkishore, D. A. Huse, and S. Sondhi, "Rare region effects dominate weakly disordered three-dimensional Dirac points," Phys. Rev. B **89**, 245110 (2014).
[55]T. Holder, C.-W. Huang, and P. M. Ostrovsky, "Electronic properties of disordered Weyl semimetals at charge neutrality," Phys. Rev. B **96**, 174205 (2017).
[56]J. Pixley, D. A. Huse, and S. Das Sarma, "Rare-region-induced avoided quantum criticality in disordered three-dimensional Dirac and Weyl semimetals," Phys. Rev. X **6**, 021042 (2016).
[57]A. Rice, J. Nelson, C. Brooks, S. Lany, and K. Alberi, "Extrinsic n-type doping of Cd_3As_2 thin films," Appl. Phys. Lett. **122**, 061901 (2023).
[58]A. Bedoya-Pinto, A. K. Pandeya, D. Liu, H. Deniz, K. Chang, H. Tan, H. Han, J. Jena, I. Kostanovskiy, and S. S. Parkin, "Realization of epitaxial NbP and TaP Weyl semimetal thin films," ACS Nano **14**, 4405–4413 (2020).
[59]M. M. Parish and P. B. Littlewood, "Classical magnetotransport in inhomogeneous conductors," Phys. Rev. B **72**, 094417 (2005).
[60]F. Kisslinger, C. Ott, and H. B. Weber, "Origin of nonsaturating linear magnetoresistance," Phys. Rev. B **95**, 024204 (2017).
[61]J. Xu, F. Han, T.-T. Wang, L. R. Thoutam, S. E. Pate, M. Li, X. Zhang, Y.-L. Wang, R. Fotovat, U. Welp, X. Zhou, W.-K. Kwok, D. Y. Chung, M. G. Kanatzidis, and Z.-L. Xiao, "Extended Kohler's rule of magnetoresistance," Phys. Rev. X **11**, 041029 (2021).
[62]J. Gao, A. Cupolillo, S. Nappini, F. Bondino, R. Edla, V. Fabio, R. Sankar, Y.-W. Zhang, G. Chiarello, and A. Politano, "Surface reconstruction, oxidation mechanism, and stability of Cd_3As_2," Adv. Funct. Mater. **29**, 1900965 (2019).
[63]A. Politano, G. Chiarello, Z. Li, V. Fabio, L. Wang, L. Guo, X. Chen, and D. W. Boukhvalov, "Toward the effective exploitation of topological phases of matter in catalysis: Chemical reactions at the surfaces of NbAs and TaAs Weyl semimetals," Adv. Funct. Mater. **28**, 1800511 (2018).
[64]L. Galletti, T. Schumann, T. E. Mates, and S. Stemmer, "Nitrogen surface passivation of the Dirac semimetal Cd_3As_2," Phys. Rev. Mater. **2**, 124202 (2018).
[65]S. Kumar, Y.-H. Tu, S. Luo, N. A. Lanzillo, T.-R. Chang, G. Liang, R. Sundararamen, H. Lin, and C.-T. Chen, "Surface-dominated conductance scaling in Weyl semimetal NbAs," npj Comput. Mater. **10**, 84 (2024).